Weather Clim. Dynam., 5, 1457–1472, 2024
https://doi.org/10.5194/wcd-5-1457-2024

Weather and Climate Dynamics
Open Access
EGU

Dynamic and thermodynamic contribution to the October 2019 exceptional rainfall in western central Africa

Kevin Kenfack[1], Francesco Marra[3], Zéphirin Yepdo Djomou[1,2], Lucie Angennes Djiotang Tchotchou[1], Alain Tchio Tamoffo[4], and Derbetini Appolinaire Vondou[1]

[1]Laboratory for Environmental Modelling and Atmospheric Physics (LEMAP), Department of Physics, University of Yaoundé 1, Yaoundé, Cameroon
[2]National Institute of Cartography, Yaoundé, Cameroon
[3]Department of Geosciences, University of Padua, Padua, Italy
[4]Climate Service Center Germany (GERICS), Helmholtz-Zentrum Hereon, Fischertwiete 1, 20095 Hamburg, Germany

Correspondence: Kevin Kenfack (kevinkenfack46@gmail.com)

Received: 27 April 2024 – Discussion started: 6 May 2024
Revised: 27 August 2024 – Accepted: 13 September 2024 – Published: 12 November 2024

Abstract. Exceptional rainfall hit western central Africa in October 2019. To understand its underlying mechanisms, we examined the regional moisture and moist static energy (MSE) budgets, intending to highlight the importance of the dynamic and thermodynamic effects associated with this historic event. Analysis of the moisture budget reveals that the precipitation anomalies in October were mainly controlled by dynamic effects. Horizontal moisture advection induced by horizontal wind anomalies controls extreme precipitation north of western central Africa, while vertical moisture advection induced by vertical velocity anomalies controls extreme precipitation south of western central Africa. Changes in the thermodynamic effect, although not the key factor responsible for the events of October 2019, contribute up to 35 % of the total effect on the northern part and 15 % on the southern part of the domain. The residual term on the northern part is important and provides a caveat when estimating dynamic and thermodynamic processes. Diagnosis of the MSE balance averaged over the northern part of western central Africa shows that the anomalous vertical motion is dominated by the dynamic effect, i.e., the wet enthalpy advection induced by the horizontal wind anomalies. This is confirmed by the high spatial correlation ($r = 0.6$) between the two terms compared to the other terms, whereas to the west of the Congo Basin, the increase in the net energy balance dominated the changes in vertical motion ($r = 0.51$). The horizontal advection of the MSE induced by the anomalies of the wet enthalpy and the vertical advection of the MSE induced by the anomalies of the MSE seem less important ($r = 0.29$ and -0.19 to the north and -0.17 and 0.03 to the south). The strong anomalies in the MSE balance in the north are linked to its meridional component, in particular the meridional wind anomalies in the dynamic effect and the meridional anomalies in latent heat in the thermodynamic effect. Our results suggest that dynamic and thermodynamic effects should be jointly considered for adequately anticipating this kind of extreme event. Understanding the associated mechanisms could help us improve our forecasts and projections and increase the region's population resilience to these extreme weather events.

1 Introduction

Equatorial Africa recorded unprecedented amounts of rainfall in October and November 2019 (Wainwright et al., 2020). Such a significant amount of precipitation is not without consequences for the population and the environment. In October, in most parts of East Africa in general, and in Kenya in particular, extreme rainfall led to flooding and landslides, provoking major destruction, with more than 100 deaths and around 18 000 people displaced internally and to neighboring countries (http://floodlist.com/africa/kenya-floods-november-2019, FloodList News, 2024). In central Africa, the Democratic Republic of the Congo was devastated by major flooding and forestry disruption along

the Congo River, forcing many people to move (Gou et al., 2022). In the Central African Republic, extreme and persistent rainfall caused significant flooding and landslides, including the Oubangui River overflowing along nearly 60 km of its coastline (Moudi et al., 2023). In addition, the night of 27 to 28 October 2019 was disastrous in the West Region of Cameroon, mainly in the locality of Bafoussam, where extreme rainfall for about 36 h caused a landslide that resulted in significant material damage with 45 dead and others missing (Aretouyap et al., 2021; Ngandam Mfondoum et al., 2021; Wantim et al., 2023). The episode was associated with a thermal depression over the Sahara and with anomalously high sea surface temperatures (SSTs). The occurrence of these conditions may change in response to anthropogenic global warming, raising the question of whether devastating events such as the one of October 2019 could occur more frequently in the future (Nicholson et al., 2022). In particular, given that climate models predict an increasing trend in extreme rainfall in the region (Fotso-Nguemo et al., 2018, 2019; Sonkoué et al., 2018; Tamoffo et al., 2019, 2023a) and that extreme precipitation in the region is associated with vegetation dynamics (Zhou et al., 2014; Mariotti et al., 2014; Marra et al., 2022; Garcin et al., 2018), it is crucial to understand the thermodynamic and dynamic mechanisms underlying these exceptional events of October 2019.

Recent studies have attempted to investigate the causes of extreme rainfall during the exceptional period of October 2019 in equatorial Africa. Nicholson et al. (2022) showed that the heavy rainfall on the Guinean coast was reinforced by positive sea surface temperature anomalies along the Atlantic coast. This process leads to significant advection of the moisture flux from the Atlantic, which, combined with the convergence of the moisture, contributed to the increase in rainfall in the region (Pokam et al., 2011; Kuete et al., 2019). Wainwright et al. (2020) pointed out that the increase in rainfall over East Africa was a consequence of the positive phase of the Indian Ocean Dipole (IOD). Indeed, Black et al. (2005) reported that during periods of the year when the dipole mode index (DMI) IOD events are greater than 0.5 °C over a period of 3 consecutive months and when the zonal SST gradient is reversed over several months, the resulting increase in rainfall over East Africa is important. In addition, the positive IOD event of 2019 lasted from late summer through to December, influencing rainfall over East Africa.

Rainfall variability in central Africa is highly dependent on the convergence of atmospheric moisture (Pokam et al., 2011; Washington et al., 2013; Dyer et al., 2017; Hua et al., 2019; Taguela et al., 2022; Tamoffo et al., 2023b, 2024). Under the effect of global warming, the increase in extreme precipitation is a consequence of the increase in available atmospheric humidity (Nicholson et al., 2022). Although previous studies have focused on analyzing meteorological factors, there is still a general lack of knowledge about quantifying the dynamic and thermodynamic effects associated with these extremes of precipitation. In recent years, the decomposition of the water balance behind precipitation anomalies is often used to isolate the dynamic and thermodynamic contributions to extreme events (Li et al., 2017; Oueslati et al., 2019; Wen et al., 2022; Kenfack et al., 2023, 2024). Water balance analysis has proved to be a useful tool for understanding anomaly fields in mean precipitation under the influence of global warming (Seager et al., 2010). In particular, moist static energy (MSE) is a useful parameter for investigating the contribution of atmospheric moisture and analyzing vertical velocity (Wang and Li, 2020a, b; Bell et al., 2015; Neelin, 2021; Nana et al., 2023; Andrews et al., 2023; Longandjo and Rouault, 2024; Kenfack et al., 2024). Recently, Kenfack et al. (2024) showed that, in the Congo Basin, the structure of the horizontal moisture advection anomalies is similar to that of the MSE advection anomalies during rainy seasons March–April–May (MAM) and September–October–November (SON). In addition, the atmospheric heating source has been identified as an indicator of precipitation (He et al., 2021). The increase in diabatic heating on the coast can contribute to the acceleration of near-surface winds (Pokam et al., 2014). An increase in this regard implies an increase in latent warming, associated with a strong ocean–continent horizontal moisture gradient, which can lead to a strengthening of the boundary layer MSE, with a positive feedback process leading to extreme precipitation. Further, it has been demonstrated that a simultaneous reduction in the heating source and rainfall has been observed in reanalyses over recent decades in the Congo Basin (Kenfack et al., 2024). Given the highlighted importance of moisture, MSE and heating sources on rainfall variability, in this study we adopt an approach based on diabatic heating, water balance and MSE to diagnose dynamic and thermodynamic processes associated with the October 2019 rainfall extremes over western central Africa.

The remainder of the paper is structured as follows. A description of the observation and reanalysis data and of the analysis methods is presented in Sect. 2. Section 3 describes the diabatic heating source and the performance of the reanalysis in capturing the October 2019 precipitation extremes. In Sect. 4, we investigate the dynamic and thermodynamic effects associated with the moisture balance. The analysis of the dynamic and thermodynamic effects associated with the MSE budget during the October 2019 rainfall anomaly period over western central Africa is presented in Sect. 5. Section 6 presents conclusions and discussions.

2 Data and methods

2.1 Data

In this study, datasets from the fifth version of the European Centre for Medium-Range Weather Forecasts reanalysis, known as ERA5 (Hersbach et al., 2020), are used for the analyses. Johannsen et al. (2019) established that over

equatorial Africa, ERA5 significantly improves upon ERA-Interim (which represents the previous dataset), particularly in the description of the hydrological cycle. In addition, Cook and Vizy (2021) have shown that ERA5 represents the spatial distribution of precipitation and atmospheric dynamic fields well compared with previous generations, particularly over the Congo Basin. With a spatial resolution of $0.25° \times 0.25°$, ERA5 is a global reanalysis dataset available from 1979 to the present, covering 137 pressure levels from the surface to 0.01 hPa. Monthly variables including horizontal and vertical wind components, geopotential, evaporation, humidity, heat flux, and temperature are used in this study. For all variables, anomalies are obtained by removing the 30-year mean of the period 1988 to 2017. In order to reinforce the robustness of the results, several variables, such as winds (horizontal and vertical), specific humidity, precipitation and evaporation, obtained from the Modern-Era Retrospective analysis for Research and Applications, version 2 (MERRA-2), which provides data from 1980 to the present day (Gelaro et al., 2017), were used in this study. To assess ERA5's ability to detect October 2019 precipitation extremes, we used three observational datasets, including rain gauge products and gauge-adjusted satellite products: the Climate Hazards Group InfraRed Precipitation with Station data (CHIRPS) gridded dataset, available at a resolution of $0.05° \times 0.05°$ (Funk et al., 2015); the Global Precipitation Climatology Project (GPCP v2.2) with a grid spacing of $2.5° \times 2.5°$ (Huffman et al., 2009); and the Climatic Research Unit (CRU TS4.03) gridded data at a resolution of $0.5° \times 0.5°$ (Harris et al., 2020).

2.2 Methods

2.2.1 Diabetic heating

Apparent diabatic heating as proposed by Yanai and Tomita (1998) and Pokam et al. (2014) is defined as follows:

$$Q = \chi \left(\frac{\partial \theta}{\partial t} + u \frac{\partial \theta}{\partial x} + v \frac{\partial \theta}{\partial y} + \omega \frac{\partial \theta}{\partial p} \right), \quad (1)$$

$$\chi = C_\mathrm{p} \left(\frac{T}{\theta} \right). \quad (2)$$

In Eqs. (1) and (2), C_p ($1005\,\mathrm{J\,kg^{-1}\,K^{-1}}$) denotes the specific heat at constant pressure, θ is the potential temperature, ω is the vertical velocity ($\mathrm{hPa\,s^{-1}}$) and $V = (u, v)$ is the vector of horizontal velocities. T (K) and p (hPa) represent the air temperature and the barometric pressure, respectively.

To quantify the monthly mean heating rate τ ($\mathrm{K\,d^{-1}}$) related to apparent heating, we use the following relation:

$$\tau = \left(\frac{Q}{C_\mathrm{p}} \right), \quad (3)$$

where Q is the combination of heat from radiation, latent heat from condensation and the convergence of the vertical vortical transport of sensible heat.

2.2.2 Diagnosis of the moisture budget

The moisture budget used to quantify the contributions of evaporation and the horizontal and vertical components associated with the circulation of moist air in the atmosphere (Seager et al., 2010; Oueslati et al., 2019; Jiang et al., 2020; Moon and Ha, 2020; Wen et al., 2022; Zhao et al., 2022; Sheng et al., 2023; Kenfack et al., 2024) is defined as follows:

$$\langle \partial_t q \rangle + \langle V \cdot \nabla_h q \rangle + \langle \omega \cdot \partial_\mathrm{p} q \rangle = E - P. \quad (4)$$

In Eq. (4), q represents the specific humidity, $V = (u, v)$ denotes the horizontal wind and ω denotes the vertical pressure velocity. E denotes surface evaporation and P precipitation. Angle brackets "$\langle\rangle$" signify the mass integral from the surface ($p_\mathrm{s} = 1000\,\mathrm{hPa}$) to a pressure $p_\mathrm{t} = 300\,\mathrm{hPa}$, which represents the top of the atmosphere layer considered. The first term on the left of Eq. (4) can be neglected given its small variation over time on a monthly scale and could contribute to the residuals (Wen et al., 2022; Sheng et al., 2023). To estimate the horizontal and vertical moisture advection components, we decompose Eq. (4) into its different linear and residual terms as follows:

$$P' = E' - \langle \overline{V} \cdot \nabla q' \rangle - \langle V' \cdot \nabla \overline{q} \rangle - \langle \overline{\omega} \partial_\mathrm{p} q' \rangle - \langle \omega' \partial_\mathrm{p} \overline{q} \rangle + \mathrm{Res}. \quad (5)$$

In Eq. (5), the overbar indicates the monthly mean climatology from 1988 to 2017 and primes indicate deviations from this climatology; the residual term "Res" contains the non-linear and transient processes associated with the joint variations in water vapor content and circulation. The terms $\langle -V' \cdot \nabla \overline{q} \rangle$ and $\langle -\omega' \partial_\mathrm{p} \overline{q} \rangle$ represent the dynamic contributions (or effect) and refer to the moisture advection induced by the horizontal wind and by the vertical pressure velocity, respectively. The terms $\langle -\overline{V} \cdot \nabla q' \rangle$ and $\langle -\overline{V} \cdot \nabla q' \rangle$ represent the thermodynamic contributions (or effect) and refer to the contribution of water vapor.

2.2.3 Diagnosis of the MSE budget

The MSE equation is defined as follows:

$$\langle \partial_t \left(C_\mathrm{v} T + L_\mathrm{v} q \right) \rangle + \langle V \cdot \nabla M \rangle + \langle \omega \partial_P m \rangle = F_\mathrm{net}, \quad (6)$$

where the moist enthalpy is

$$M = C_\mathrm{p} T + L_\mathrm{v} q \quad (7)$$

and the MSE is

$$m = C_\mathrm{p} T + L_\mathrm{v} q + \Psi. \quad (8)$$

In Eqs. (6)–(8), $C_\mathrm{p}(C_\mathrm{v})$ represents the specific heat at constant pressure (the specific heat at constant volume), T is the air temperature and Ψ is the geopotential. F_net is the net energy entering the atmospheric column at the surface and

top of the atmosphere (latent heat, sum of sensible heat, and shortwave and longwave radiative fluxes). Similarly to the moisture flux equation, the first term on the left of Eq. (6) can be neglected given its small variation over time on a monthly scale and it contributing to the residuals. In addition, it should be noted that variations in geopotential height along pressure levels are neglected in this formulation of the MSE budget. The remaining terms in Eq. (6) can be decomposed into horizontal and vertical advection components, as described by

$$\langle \omega' \partial_p \overline{m} \rangle = -\langle \overline{V} \cdot \nabla M' \rangle - \langle V' \cdot \nabla \overline{M} \rangle - \langle \omega \partial_p m' \rangle + F'_{\text{net}} + \text{Res.} \quad (9)$$

Anomalous vertical motion is analyzed using this equation with a given profile of $\overline{m}$. Similarly to the convention adopted for decomposing the moisture flux, the term $-\langle V' \cdot \nabla \overline{M} \rangle$ relates to the anomalous MSE associated with the atmospheric circulation and contains the dynamic contribution (or effect), while the two terms $-\langle \overline{V} \cdot \nabla M' \rangle$ and $-\langle \omega \partial_p m' \rangle$ refer to the thermodynamic contribution (or effect), which is crucial for diagnosing the thermal state of the atmosphere associated with the increase in the vertical rise of the air.

3 Diabatic heating and extreme rainfall

The increase in SSTs in the eastern Atlantic (Fig. 1a) has been identified as one of the causes of the positive precipitation anomalies over western central Africa in October 2019. The warming contrast between the ocean and the continent favored the strengthening of the moisture advection associated with the precipitation anomalies over western central Africa (Fig. 1b). This is in agreement with Nicholson et al. (2022).

Figure 2 represents the mean vertical profile (pressure-latitude) of diabatic heating averaged between 6° and 20° E during SON for the 1988–2017 climatology (Fig. 2a) and the corresponding profile for 2019 (Fig. 2b). During SON, the main source of heat is located between 3° S and 9° N for climatology and between 5° S and 13° N for 2019.

However, 2019 presents a more extensive and pronounced source of heat compared with the climatology of 1988–2017. A 3–4 K d^{-1} heating rate, more intense in 2019, occurred from 600 hPa. A cooling rate of 1–2 K d^{-1} took place around 850 hPa in the south and from 550 hPa in the north. The profound heating observed from 600 hPa originates at the surface in the southern portion of the domain (10° S). It is reinforced by the contrast between the large positive values and the negative values on either side of the Equator between 500 and 400 hPa. The vertical structure of the divergent circulation is also illustrated in Fig. 2. The divergent circulation appears more pronounced from 550 hPa in 2019 (Fig. 2b) compared with the climatology of 1988–2017 (Fig. 2a). This is consistent with the warming contrast observed. This uplift was reinforced by the warming of the equatorial Atlantic associated with an abnormally strong thermal low over the Sahara, which led to an acceleration of the dominant meridional flow in the divergent circulation (Fig. 2c). This is in agreement with Nicholson et al. (2022), who highlighted that the West African monsoon was late to withdraw in 2019.

Although the SON season has shown significant diabatic heating compared to climatology, October 2019 in particular over western central Africa recorded extremes of rainfall (Nicholson et al., 2022). In this study, we use the ERA5 precipitation fields for water balance analysis. This ensures that all the examined physical quantities are consistent across the study. Before doing so, we assessed the performance of ERA5 in detecting the extreme precipitation events in October 2019. Figure 3 illustrates the interannual variability in October rainfall anomalies over western central Africa for the period 1987–2021.

ERA5 (red) and the CHIRPS (blue), GPCP (maroon) and CRU (black) observations are consistent in highlighting the high-precipitation peak of 2019. CHIRPS shows the highest values of positive anomalies of up to 3.5 mm d^{-1}, while ERA5 shows values of up to 2.5 mm d^{-1}. Despite some differences between ERA5 and the observations in representing trends on an interannual scale (Kenfack et al., 2024), the unprecedented event of October 2019 was well detected. In addition, the exceptional event is also detected by the MERRA-2 reanalysis (Fig. S1).

The increase in SSTs in the tropical Atlantic reached a record level in October 2019 (Nicholson et al., 2022). This may have resulted in increased specific humidity over land. Figure 4 depicts the vertical profile (pressure level–latitude) of specific humidity (colors) and meridional wind (contours) averaged between 6° and 20° E for the 1988–2017 climatology (Fig. 4a), the October 2019 average (Fig. 4b) and the October 2019 anomaly (Fig. 4c).

The 1988–2017 climatology is characterized by intense surface specific humidity extending as far as 12° N, whereas the October 2019 average appears to extend further to 15° N. In addition, the southerly wind in 2019 was more pronounced up to 15° N compared to the climatology. Analysis of the anomalies confirms that the humidity extended further north in western central Africa in October 2019 compared with the climatology. The intensification of the southerly wind up to 15° N indicates that this moisture probably comes from the equatorial Atlantic. This is in agreement with Kamae et al. (2017), who highlighted that extreme precipitation can be a consequence of changes in humidity. Indeed, the increase in humidity associated with a substantial heating source contributes to an increase in precipitation.

4 Moisture budget analysis

Rainfall variability in equatorial central Africa is strongly dependent on the moisture inputs associated with atmospheric circulation (Jackson et al., 2009; Cook and Vizy, 2019, 2021; Dyer et al., 2017; Longandjo and Rouault, 2024). In the Congo Basin, atmospheric heating sources combined with

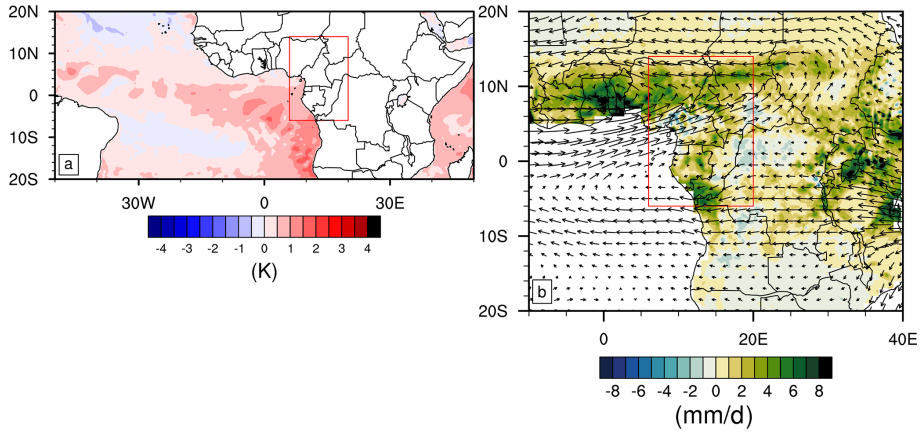

Figure 1. SST **(a)** and rainfall **(b)** anomalies during October 2019. The vectors represent anomalies of vertically integrated atmospheric moisture flux. The red box indicates the western central Africa area.

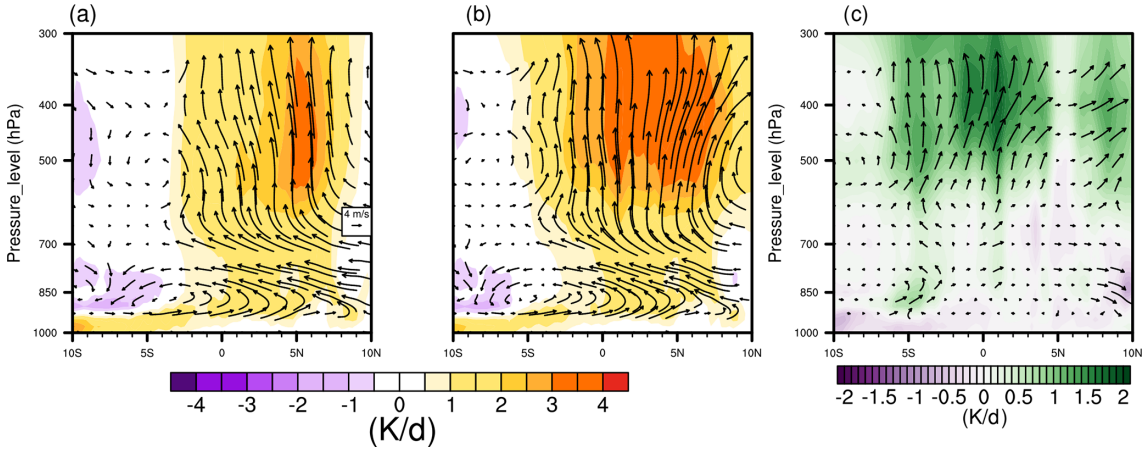

Figure 2. Diabatic heating and divergent meridional circulation (vectors; $\mathrm{m\,s^{-1}}$) during the SON season for the **(a)** 1988–2017 avg, **(b)** 2019 avg and **(c)** anomaly, all averaged between 6 and 20° E. As the vertical velocity is much weaker than the meridional wind, its values have been enhanced by a factor of 600 for the clarity of the graph.

the vertical advection of moisture induced by anomalous vertical motion are responsible for most of the interannual variability in precipitation (Kenfack et al., 2024). In this section, we decompose the moisture budget in Eq. (5) to examine the processes that led to the October 2019 extreme rainfall over western central Africa. To do this, we analyze local variations in rainfall associated with atmospheric moisture introduced into the air column by atmospheric circulation.

The monthly anomalies of the different components of the water balance averaged over the northern part of western central Africa (6–14° N, 6–20° E) for the month of October 2019 (Fig. 5a) indicate that the increase in dynamic processes dominated the increase in precipitation. Horizontal advection of moisture induced by the horizontal wind anomaly $\langle -V' \cdot \nabla \overline{q} \rangle$ was the most pronounced component (up to 2.5 $\mathrm{mm\,d^{-1}}$). Although thermodynamic processes $\langle -\overline{V} \cdot \nabla q' \rangle$ and $\langle -\overline{\omega} \partial_p q' \rangle$ are weaker than dynamic processes, they also contributed to the extreme rainfall amounts. Evaporation E, for its part, contributed very little (0.1 $\mathrm{mm\,d^{-1}}$). This is consistent with Cook et al. (2019), who found that rainfall anomalies in equatorial central Africa do not depend directly on surface heating. It should also be noted that the residual term for a value of $-1.2\,\mathrm{mm\,d^{-1}}$ is considerable. Indeed, the northward shift and strengthening of the northern component of the African easterly jet (AEJ-N) in October are verified (Nicholson et al., 2022). This is illustrated by the anomalous 700 hPa zonal wind in October 2019. In addition, the anomalous variance of the band-pass-filtered 700 hPa meridional wind over 2–6 d is also visible, indicating African easterly wave activity (Reed et al., 1977). Other studies also point out that rainfall fluctuations in equatorial Africa are associated with Kelvin waves (Jackson et al., 2009). The residual term could influence the estimation of dynamic and thermodynamic distributions in the water budget, and its high values in the Sahel region would be associated with a nonlinear interaction between wind and changes in humidity.

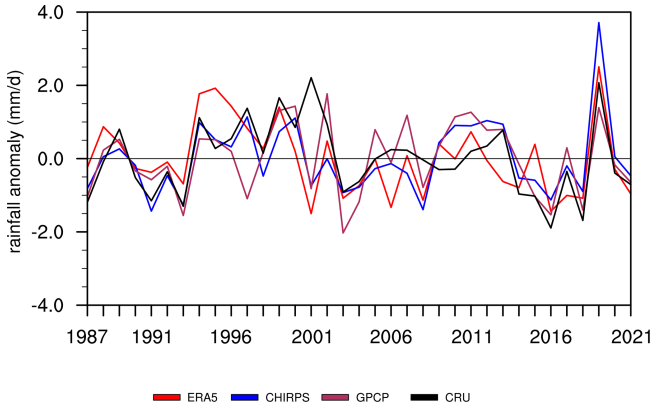

Figure 3. Temporal evolution of the October rainfall anomaly over western central Africa (6° S–14° N, 6–20° E), from reanalysis data ERA5 (red) and from observational data CHIRPS (blue), GPCP (maroon) and CRU (black), covering the period 1987–2021.

Analysis of the components of the water balance over the western part of the Congo Basin (6° S–5° N, 6–20° E) for October 2019 (Fig. 5b) shows that the increase in rainfall was dominated by vertical advection of moisture induced by changes in vertical velocity $\langle -\omega' \partial_p \overline{q} \rangle$ ($1.4\,\mathrm{mm\,d^{-1}}$). However, the contributions of the other processes, including the residual term, are low.

At the pixel scale, positive precipitation anomalies over eastern Nigeria, southern Chad and northern Cameroon (Fig. 6a) were mainly dominated by horizontal moisture advection induced by the horizontal wind anomaly (Fig. 6d). Over Gabon, south of Congo (Brazzaville), positive precipitation anomalies were dominated by vertical moisture advection induced by vertical anomalous motion (Fig. 6f). Horizontal moisture advection induced by the specific humidity anomaly (Fig. 6c), although not the key factor associated with precipitation patterns, shows a small positive contribution over the northern part of the domain.

The contribution of evaporation (Fig. 6b) and horizontal advection of moisture induced by the specific humidity anomaly (Fig. 6e) remains weak over the entire domain, although some positive values can be seen around 14° N. This result is similar to that provided by MERRA-2 (Fig. S2). Thermodynamic effects reflect the change in the thermal state of the atmosphere associated with the October 2019 rainfall extremes over western central Africa. However, changes in the thermodynamic effect, although not the key factor responsible for the October 2019 events, contributed up to 35 % of the total effect (the sum of dynamic and thermodynamic contributions) on the northern part and 15 % on the southern part of the domain. This could be since the increase in diabatic heating contributes to the change in the thermal state of the atmosphere, i.e., the increase in thermodynamic effects (changes in humidity). In fact, Nicholson et al. (2022) reported that the increase in SST in the tropical Atlantic strengthened the advection of moist air from the Atlantic towards the region, with an increase in the moisture flux from the west to southwest.

5 MSE budget analysis

The previous results clearly showed that the vertical advection of moisture induced by the vertical velocity anomaly was identified as the second dynamic parameter (after the horizontal advection of moisture induced by the anomalous horizontal movement) contributing to the increase in precipitation in October 2019. Diagnosis of the MSE budget, which takes account of the thermal state of the atmosphere and the effect of atmospheric circulation, is used to analyze the atmospheric perturbation related to moisture transport. The MSE largely influences the structure of vertical motion. In addition, diagnosis of the MSE balance emphasizes the relative contributions of temperature, specific humidity and atmospheric circulation associated with the vertical motion anomaly.

The vertical profiles of the vertical velocity anomaly ω' and the MSE climatology $\overline{m}$ averaged over the north of the domain are shown in Fig. 7a. The vertical velocity anomaly ω' shows positive values at the surface and negative values in the middle and upper troposphere. The alternation of positive and negative values in the tropospheric column probably reduces the contribution of the vertical advection of moisture induced by the anomalous vertical motion. The MSE climatology $\overline{m}$ exhibits a bottom-heavy structure with a minimum around 650 hPa. Such a structure generally indicates that $\langle \partial_p \overline{m} \rangle < 0$ (Chen and Bordoni, 2014; Liu et al., 2021; Wen et al., 2022). As a result, positive (negative) values of $\langle \omega' \partial_p \overline{m} \rangle$ depend on the vertical structure of the omega anomalies. The vertical velocity climatology $\overline{\omega}$ (Fig. 7b) is negative over the entire troposphere, characterizing an upward movement. The MSE anomaly m' decreased slightly near the surface and then increased from 800 to 550 hPa, with a minimum value around 550 hPa. However, this includes three terms, namely, gz', which is weak in the entire tropospheric column; the enthalpy anomaly $C_p T'$, which tends to increase; and $L_v q'$, which tends to behave similarly to m' between 650 hPa and 300 hPa. To the south of the domain (Fig. 7c), the vertical velocity anomaly shows negative values from 900 hPa up to the upper troposphere, accelerating the anomalous vertical movement. The structure of the MSE climatology is similar to that observed to the north, with a maximum of around 650 hPa. The vertical profiles (Fig. 7d) of the MSE anomaly and the latent energy anomaly show similar structures throughout the tropospheric column, with maximum values at 650 hPa.

Based on the contributions of the different terms in Eq. (9) to the MSE over the northern part of western central Africa (Fig. 8a), the advection of wet enthalpy induced by the horizontal wind anomalies $-\langle V' \cdot \nabla \overline{M} \rangle$ is the main term contributing most to the vertical advection of the MSE induced

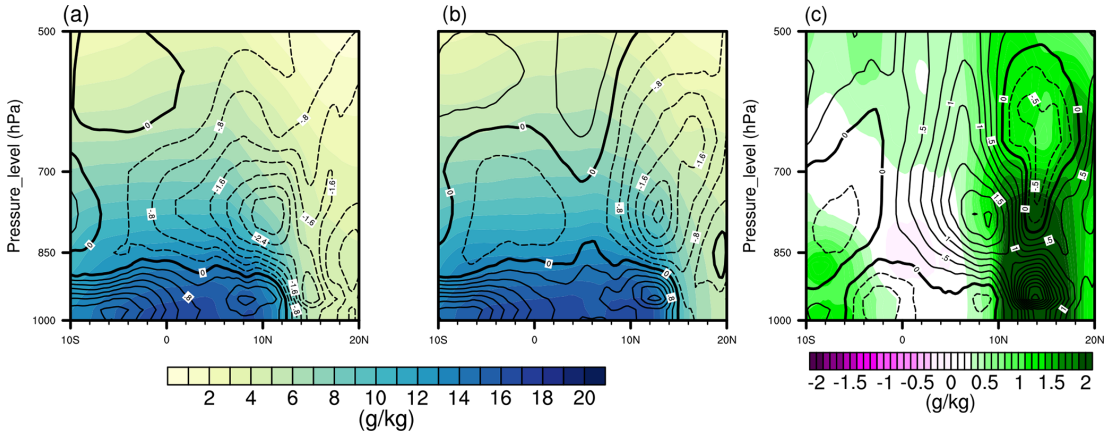

Figure 4. Specific humidity and meridional wind (contours: $\mathrm{m\,s^{-1}}$) in October for the **(a)** 1988–2017 avg, **(b)** 2019 avg and **(c)** anomaly, averaged between 6–20° E.

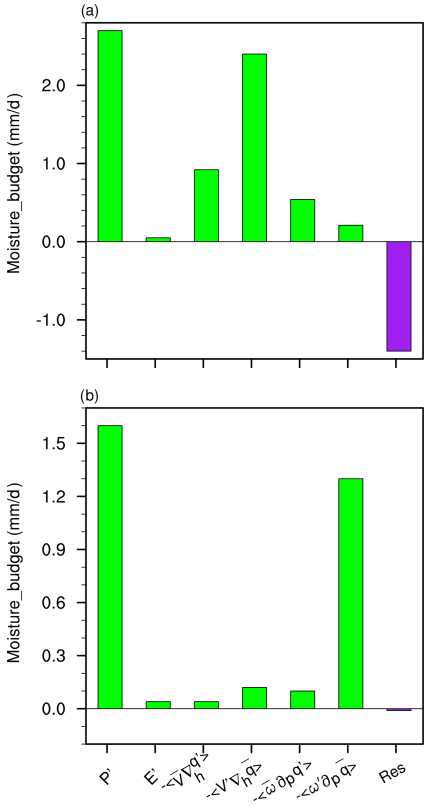

Figure 5. Monthly mean anomalies in the moisture budget for October 2019, averaged **(a)** over the northern part of western central Africa (6–14° N, 6–20° E) and **(b)** over the southern part of western central Africa (6° S–5° N, 6–20° E).

by the vertical velocity anomaly $\langle \omega' \partial_p \overline{m} \rangle$. This is confirmed by the high correlation ($r = 0.6$) between the two terms compared to the other terms.

We also note the contribution of the thermodynamic terms, although the horizontal advection of the MSE induced by the wet enthalpy variation $-\langle \overline{V} \cdot \nabla M' \rangle$ dominates ($r = 0.3$) compared to the vertical advection of the MSE induced by the MSE variation $-\langle \omega \partial_p m' \rangle$ ($r = -0.2$). A weak contribution from the net flow of energy is noticeable ($r = 0.18$). This could be due to the fact that the energy in the radiative and turbulent heat fluxes penetrating the atmosphere over western central Africa has suffered a loss linked to the increase in cloud cover, which has a strong influence on shortwave radiation. Such a reduction in energy in the air column has an impact on upward motion. This result is in line with that of Wen et al. (2022) and Sheng et al. (2023), who pointed to a reduction in the net energy in the air column during the exceptional rainy season in the summer of 2020 in the Yangtze River valley and the anomalous increase in precipitation over southern China in 2022. However, as with the moisture balance, the residual term is also considerable.

To the south of the domain (Fig. 8b), the increase in the net energy balance was responsible for strengthening the vertical advection of the MSE induced by the vertical velocity anomaly ($r = 0.51$).

In addition, the increase in vertical movement was reinforced by an increase in the horizontal advection of the MSE induced by the variation in wet enthalpy $-\langle \overline{V} \cdot \nabla M' \rangle$. This is in agreement with the results of Kenfack et al. (2024), who highlighted the importance of horizontal advection in the MSE and moisture flux as well as their implications for vertical motion over the Congo Basin. The contributions in vertical advection induced by changes in the MSE and horizontal advection induced by changes in the horizontal wind are small. Moreover, similarly to the moisture flux advected in the western part of the Congo Basin, the residual term was less important in the MSE budget compared to the northern part.

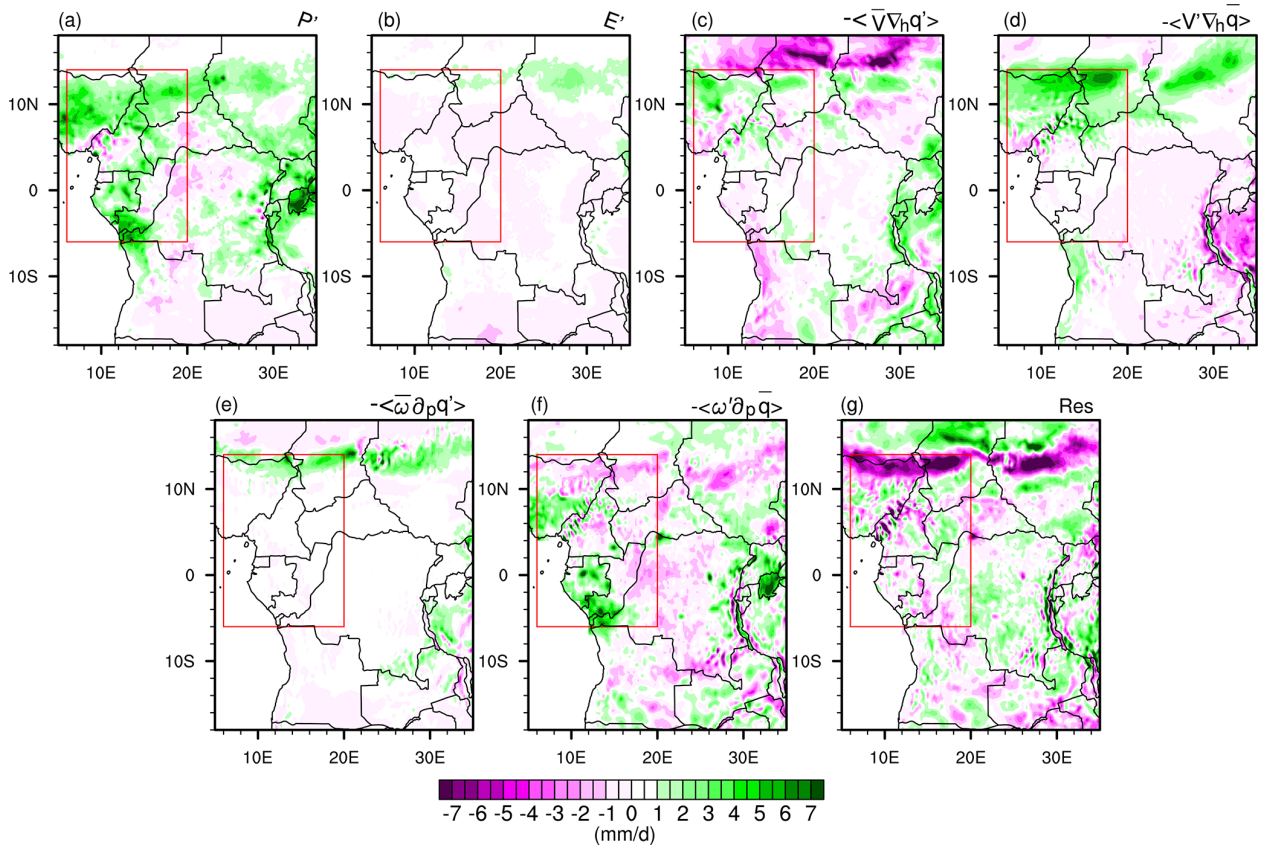

Figure 6. Spatial distributions of each term of the water budget equation during October 2019 over western central Africa (red box). **(a)** Precipitation anomaly, **(b)** evaporation anomaly, **(c)** horizontal advection of anomalous moisture by climatological wind, **(d)** horizontal advection of climatological moisture by anomalous wind, **(e)** vertical advection of anomalous moisture by climatological vertical velocity, **(f)** vertical advection of climatological moisture by anomalous vertical velocity and **(g)** the residual term.

On a regional scale, the vertical advection of the MSE induced by the vertical motion anomaly $\langle \omega' \partial_p \overline{m} \rangle$ (Fig. 9a) is mainly dominated by the dynamic term $\langle V' \cdot \nabla \overline{M} \rangle$ (Fig. 9c), which brings moist enthalpy into the domain.

There is a high concentration of positive values in both dynamic terms, up to 120 W m^{-2} in the north of western central Africa. In addition, the two thermodynamic terms $-\langle \omega \partial_p m' \rangle$ (Fig. 9b) and $-\langle \overline{V} \cdot \nabla M' \rangle$ (Fig. 9d), although weak, also contributed to reinforcing the vertical advection of MSE induced by the vertical motion anomaly. It should be remembered that the term $-\langle \omega \partial_p m' \rangle$ remains very weak over the region as a whole, except in the northern part where a slight layer of positive values can be observed. Terms $-\langle V' \cdot \nabla \overline{M} \rangle$, $-\langle \overline{V} \cdot \nabla M' \rangle$ and $-\langle \omega \partial_p m' \rangle$ in the MSE have a similar spatial distribution to terms $\langle -V' \cdot \nabla \overline{q} \rangle$, $\langle -\overline{V} \cdot \nabla q' \rangle$ and $\langle -\overline{\omega} \partial_p q' \rangle$ in the moisture, which is in agreement with the findings of Kenfack et al. (2024). The difference between the net energy balance for 2019 and the climatology (Fig. 9e) shows low positive values in the north and south of the region. Such an increase (mainly to the south of the area) is associated with a strengthening in the vertical structure of the MSE anomaly through ascending currents and, consequently, an increase in precipitation. A further analysis of the net energy balance (Fig. 10) shows that during October 2019, the latent heat flux (Fig. 10a) decreased mainly over the Sahel and to the south of the domain. Sensible heat, on the other hand, increased slightly, with values of around 1.5 W m^{-2}. Analysis of the radiative flux anomalies shows strong positive values over the Sahel and the southern part of the domain (up to 50 W m^{-2}), showing that this is the main factor responsible for the increase in the energy balance during the exceptional event of October 2019.

Although the dynamic contribution is the most important contribution, the thermodynamic contribution cannot be neglected. This would mean that the interaction between atmospheric dynamic and thermodynamic variables would induce significant indirect effects on October 2019 precipitation anomalies over western central Africa.

5.1 Dynamic effect

The aforementioned results clearly show that enthalpy advection induced by the horizontal wind anomaly is crucial in understanding the processes at the origin of October 2019 extreme precipitation over the northern part of western cen-

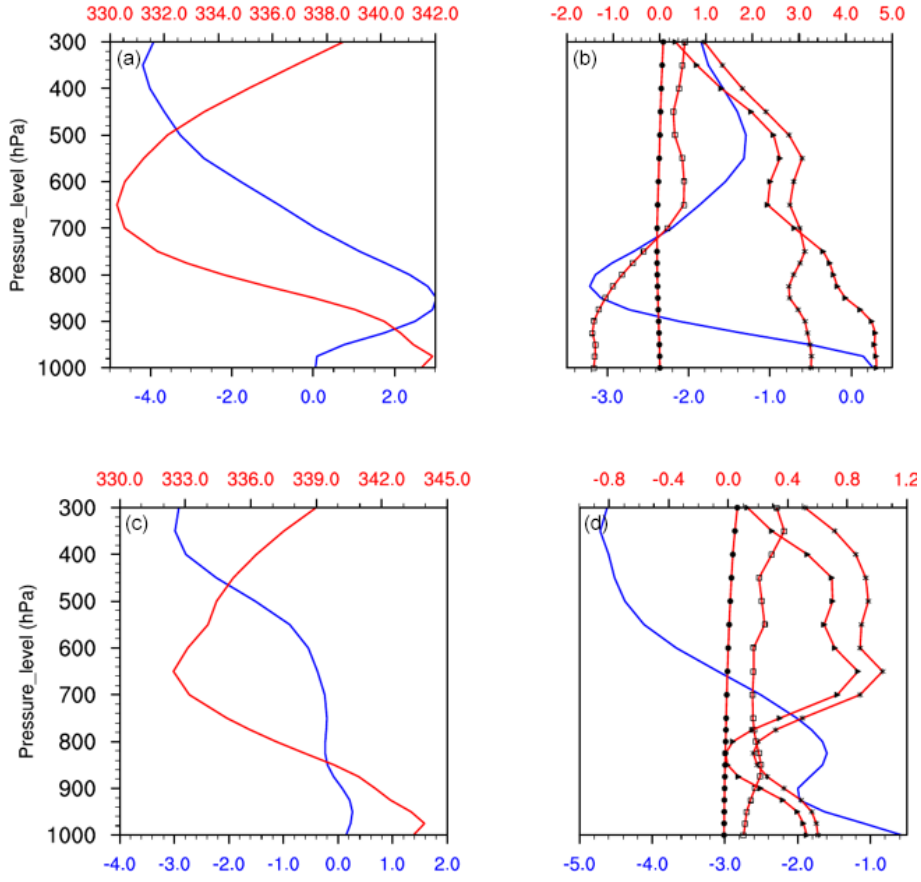

Figure 7. Vertical profile of **(a)** the vertical velocity anomaly ω' (blue line: 10^{-2} Pa s^{-1}) and MSE climatology $\overline{m}$ (red line: 10^3 J kg^{-1}) and **(b)** the vertical velocity climatology $\overline{\omega}$ (blue line: 10^{-2} Pa s^{-1}), MSE anomaly m' (line with crosses: 10^3 J kg^{-1}), enthalpy anomaly C_pT' (line with open squares: 10^3 J kg^{-1}), latent energy anomaly L_vq' (line with dark triangles: 10^3 J kg^{-1}) and geopotential anomaly Ψ' (line with dark circles: 10^3 J kg^{-1}) averaged over the northern part of western central Africa (6–14° N, 6–20° E) and **(c, d)** the same parameters averaged over the southern part of western central Africa (6° S–5° N, 6–20° E) during October 2019.

tral Africa. It should be remembered that, as we mentioned in the diagnostic section of the MSE balance, the wet enthalpy $M = C_pT + L_vq$ results from the sum of the dry enthalpy and the latent heat. Thus, the horizontal advection of wet enthalpy induced by the wind anomaly can be separated into two terms: dry enthalpy $-\langle V' \cdot \nabla_h C_p \overline{T} \rangle$ (Fig. 11a) and latent heat $-\langle V' \cdot \nabla_h L_V \overline{q} \rangle$ (Fig. 11d).

Given the influence of the wind anomaly components on the displacement of dry enthalpy and latent heat, a further decomposition of the $-\langle V' \cdot \nabla_h C_p \overline{T} \rangle$ and $-\langle V' \cdot \nabla_h L_V \overline{q} \rangle$ terms along the zonal (Fig. 11b, e) and meridional (Fig. 11c, f) directions appears to be necessary. Figure 11a shows that the advection of dry enthalpy induced by the horizontal wind anomaly decreased over the averaged area, with the highest values between 6 and 14° N. The advection of dry enthalpy by the meridional wind anomaly (Fig. 11c) is particularly responsible for the decrease in the $-\langle V' \cdot \nabla_h C_p \overline{T} \rangle$ term compared with the advection of dry enthalpy induced by the zonal wind anomaly (Fig. 11b), which is weak. For the transport of latent heat (Fig. 11d), the influence of the advection of the $-\langle V' \cdot \nabla_h L_V \overline{q} \rangle$ term under the effect of the anomalous meridional circulation is the main term responsible for the supply of moist air to the northern part of the area, while the low contribution to the south is associated with a low input of moist air from the zonal wind anomaly (Fig. 11f). Analysis of the advection of dry enthalpy and latent heat by anomalous winds shows that the meridional wind anomaly had a significant impact compared with the zonal wind anomaly. In addition, the advection of the dynamic term associated with latent heat contributed significantly to the supply of MSE to western central Africa compared to the advection of the dynamic term associated with dry enthalpy. One of the reasons for this would be because, in addition to the warm Atlantic SSTs, there was an anomalous meridional mean sea level pressure (MSLP) gradient in the central African Sahel between a lower MSLP over the eastern Sahara and a higher pressure between 10 and 15° N. In addition, the trans-equatorial meridional wind fluctuated with the activity of the African easterly waves over the Gulf of Guinea (Nicholson et al., 2022).

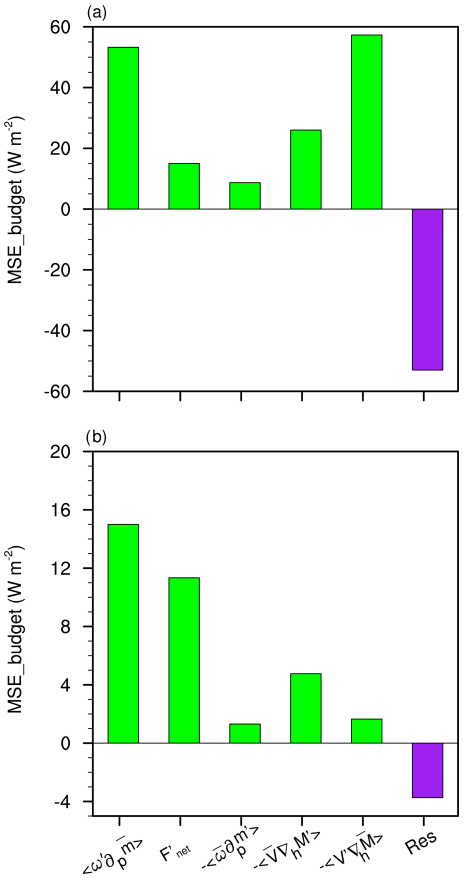

Figure 8. Different terms of the moist static energy (MSE) budget averaged **(a)** over the northern part of western central Africa (6–14° N, 6–20° E) and **(b)** over the southern part of western central Africa (6° S–5° N, 6–20° E).

5.2 Thermodynamic effect

The results of the previous section highlighted the importance of dynamics, particularly in a meridional direction, for extreme precipitation in October 2019. However, we previously also observed that the thermodynamic contribution should not be neglected. Similarly to the previous section, the thermodynamic term $-\langle \overline{V} \cdot \nabla M' \rangle$ (i.e., the advection of the wet enthalpy anomaly associated with wind climatology) can also be separated into two terms, namely dry enthalpy $-\langle \overline{V} \cdot \nabla_h C_p T' \rangle$ (Fig. 12a) and latent heat $-\langle \overline{V} \cdot \nabla_h L_V \overline{q}' \rangle$ (Fig. 12d).

To better assess the contribution of each term, we split the horizontal wind into zonal and meridional directions. The advection of the dry enthalpy anomaly by the horizontal zonal and meridional wind components is shown in Fig. 12b and c, respectively. It can also be seen that the dry enthalpy anomaly is very small over the whole area. On the other hand, the advection of the latent heat anomaly by the horizontal wind climatology is more pronounced. Variations in latent heat are strong in the meridional direction, while the zonal direction shows a reduction in abnormal latent heat. This could be due to the strong meridional wind associated with the increase in SST in the tropical Atlantic, which results in strong advection of water vapor into western central Africa, leading to precipitation. The reduction in the advection of the latent heat anomaly on the Atlantic coast is amplified by the zonal wind climatology. However, the advection of the wet enthalpy induced by the horizontal wind anomaly (dynamic effect) is stronger than the advection of the wet enthalpy anomaly by the wind climatology. As a result, we note in particular the changes in the meridional wind for the dynamic effect and the latent heat associated with the warming of the equatorial Atlantic for the thermodynamic effect.

6 Summary and concluding remarks

Western central Africa was hit by unprecedented exceptional rainfall in October 2019. A few studies have investigated the meteorological causes associated with these extreme rainfall events (Wainwright et al., 2020; Nicholson et al., 2022). This study followed these perspectives and focused on evaluating the dynamic and thermodynamic processes that controlled the extreme events of 2019. We proceeded by decomposing the water balance and MSE equation, separating the associated dynamic and thermodynamic effects. Changes in atmospheric circulation are behind dynamic processes, while changes in water vapor are behind thermodynamic processes. This approach provides a better understanding of the mechanisms behind rainfall anomalies. The main findings can be summarized as follows:

1. The main feature of October 2019 in the northern part of the area was a strong southerly circulation compared with the typical climatology for 1988–2017. In addition, a more pronounced rate of humidity associated with significant diabatic heating over western central Africa up to 15° N was recorded.

2. The diagnosis of the water balance reveals that the exceptional rainfall in October 2019 was mainly dominated by dynamic effects. However, moisture advection induced by horizontal wind anomalies is the dominant process of precipitation anomalies over the northern part of the zone, while vertical moisture advection induced by vertical velocity anomalies is the dominant process of precipitation extremes in the south, mainly over Gabon and southern Congo (Brazzaville). Changes in the thermodynamic effect, although not the key factor responsible for the events of October 2019, contribute up to 35 % of the total effect (the sum of the dynamic and thermodynamic contributions) on the northern part and 15 % on the southern part of the domain. The contribution of evaporation remains weak in both areas combined, which allows us to conclude that evaporation was

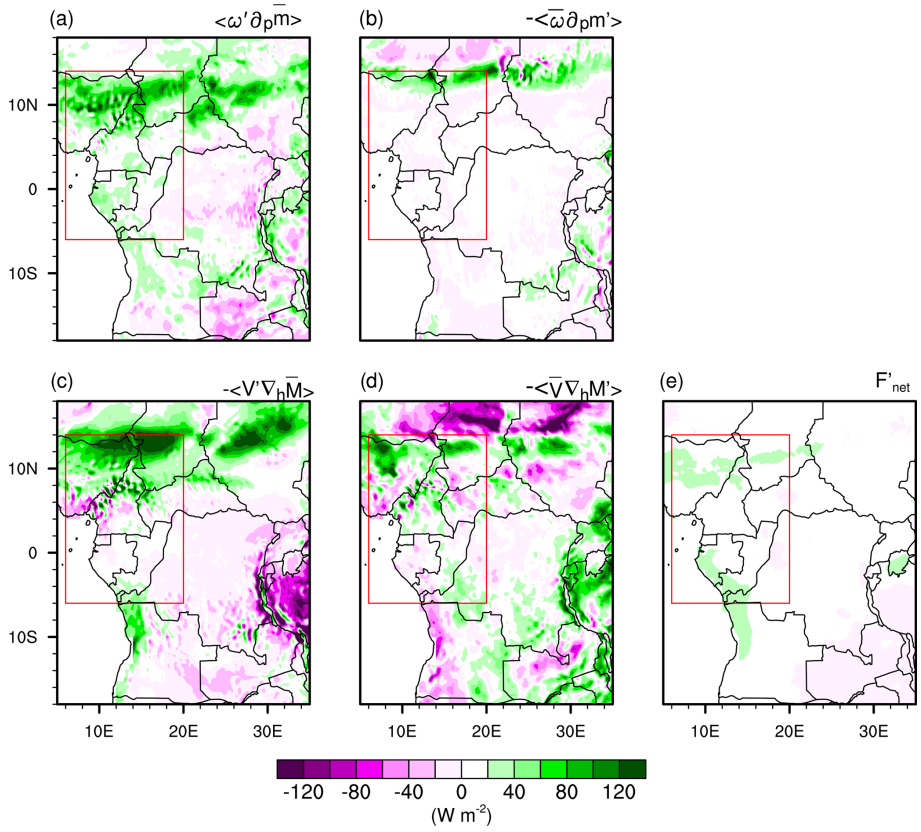

Figure 9. Spatial distributions of each term of the moist static energy (MSE) balance equation during October 2019 over western central Africa (red box). **(a)** Vertical advection of climatological MSE by anomalous vertical velocity, **(b)** vertical advection of anomalous MSE by climatological vertical velocity, **(c)** horizontal advection of anomalous moist enthalpy by climatological wind, **(d)** horizontal advection of climatological moist enthalpy by anomalous wind and **(e)** net energy flux (at the surface and top of the atmosphere) in the atmospheric column.

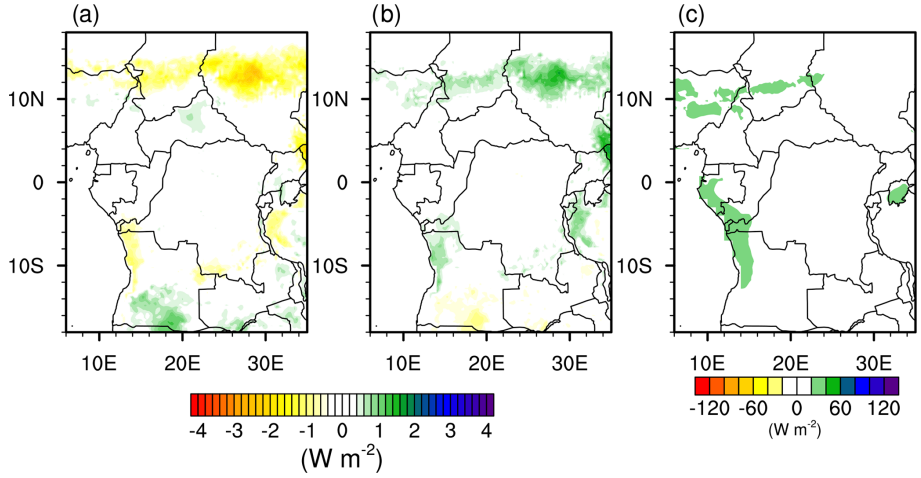

Figure 10. Spatial distribution of **(a)** latent heat, **(b)** sensible heat and **(c)** radiative flux anomalies in October 2019 over western equatorial Africa.

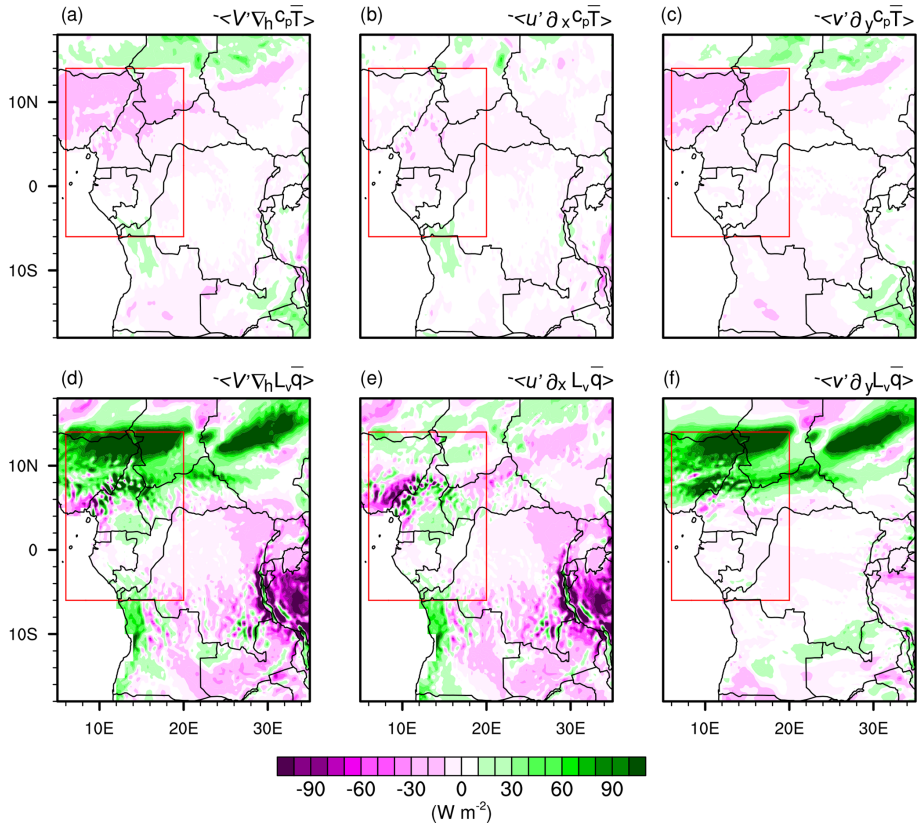

Figure 11. Horizontal advection of **(a–c)** climatological dry enthalpy and **(d–f)** latent energy by anomalous wind, designated a dynamic effect during October 2019 over western central Africa (red box). **(a, d)** Total advection, **(b, e)** the zonal component and **(c, f)** the meridional component.

not responsible for the heavy rainfall of October 2019 in western central Africa.

3. Over the northern part of the area, the MSE vertical advection anomaly is dominated by the dynamic term (i.e., the advection of the wet enthalpy induced by the horizontal wind anomalies) compared to the thermodynamic terms (i.e., the horizontal advection of the MSE induced by the variation in the wet enthalpy and the vertical advection of the MSE induced by the variation in the MSE). In the southern part, the increase in the net energy balance compared with the climatology is the dominant process that has contributed most to the change in the structure of the vertical anomaly of the MSE. The prevailing net balance is controlled by the anomalies in radiative flux compared with the anomalies in latent and sensible heat flux. An extended analysis shows that these variations in the MSE over the north of western central Africa were governed by its meridional component, in particular the variations in the meridional wind in the dynamic effect and the meridional variations in latent heat in the thermodynamic effect. It should be pointed out that in both cases, the contribution of dry enthalpy helped to reduce the dynamic term and was small in the thermodynamic term.

The results of this study show that moisture advection induced by horizontal wind anomalies and vertical moisture advection induced by vertical velocity anomaly were crucial mechanisms in the anomalous October 2019 exceptional rainfall increase over western central Africa. In addition, changes in the MSE budget, mainly through the meridional circulation (dynamic effect), and latent heat (thermodynamic effect) also played an important role in the northern part of the area, while the increase in the energy balance contributed considerably to the change in the MSE balance in the southern part of the area. However, there was little contribution from dry enthalpy. These results are consistent with those of Nicholson et al. (2022), who showed that the increase in equatorial Atlantic SSTs associated with the late retreat of the West African monsoon played an important role in precipitation anomalies in the Sahel. Changes in SSTs along the east coast of the equatorial Atlantic display a similar pattern to the Atlantic Niño as described by Lutz et al. (2013). Furthermore, Vallès-Casanova et al. (2020) also highlighted the fact that 2019 was characterized by a particularly intense Atlantic Niño, which lasted until October, placing the dynamic

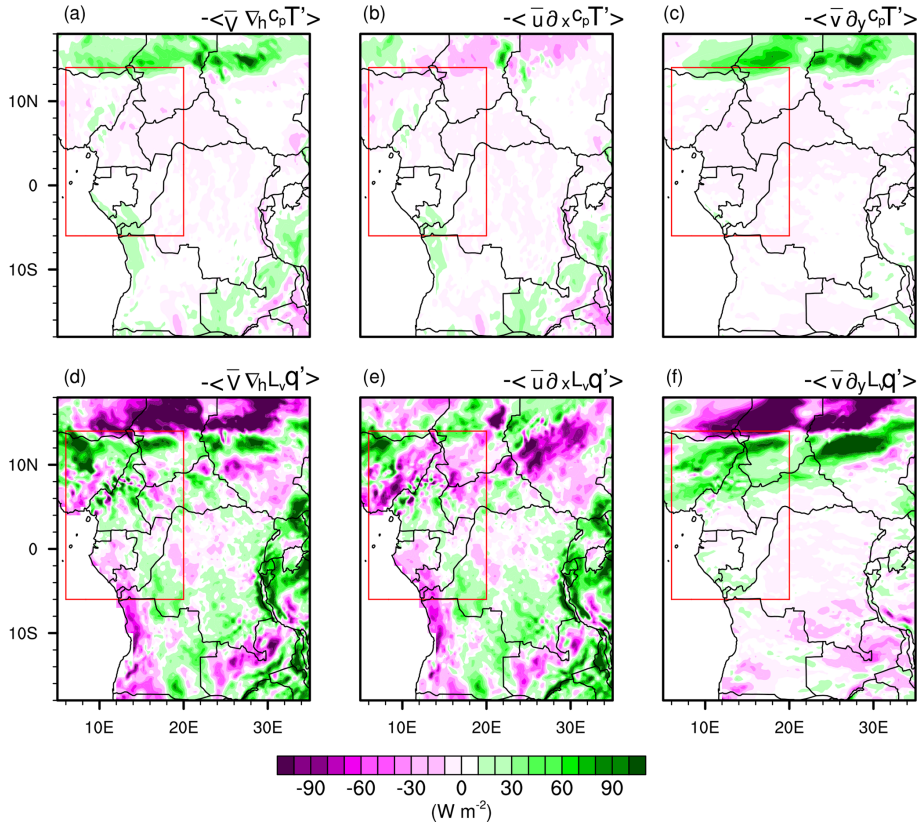

Figure 12. As in Fig. 11 but for the thermodynamic effect (horizontal advection of anomalous dry enthalpy and latent energy by climatological wind) during October 2019 over western central Africa (red box).

and thermodynamic processes in the context of the large-scale circulation. The importance of the dynamic contribution during extreme precipitation events has been reported in other regions, notably over southern China (Wen et al., 2022; Sheng et al., 2023). This calls for comprehensive evaluations of both dynamic and thermodynamic contributions, as well as their possible feedback, to assess the potential impact of climate change on extreme precipitation events in this region.

Code availability. Figures shown in this study are plotted using the NCAR Command Language (NCL; https://doi.org/10.5065/D6WD3XH5, NCAR Command Language, 2017). Codes can be obtained from the corresponding author.

Data availability. ERA5 is produced within the Copernicus Climate Change Service (C3S) by the ECMWF and is accessible via the following link: https://cds.climate.copernicus.eu/datasets/reanalysis-era5-pressure-levels-monthly-means?tab=download (C3S, 2024).

Supplement. The supplement related to this article is available online at: https://doi.org/10.5194/wcd-5-1457-2024-supplement.

Author contributions. KK: conceptualization; data analysis; formal analysis; investigation; methodology; writing – original draft; writing – review and editing. FM: supervision; conceptualization; investigation; writing – review and editing. ZYD: investigation; writing – review and editing; supervision; validation. LADT: validation; supervision; methodology; writing – review and editing. ATT: conceptualization; investigation; methodology; project administration; resources; supervision; validation; writing – review and editing. DAV: project administration; supervision; resources; validation; methodology; writing – review and editing.

Competing interests. The contact author has declared that none of the authors has any competing interests.

Disclaimer. Publisher's note: Copernicus Publications remains neutral with regard to jurisdictional claims made in the text, published maps, institutional affiliations, or any other geographical representation in this paper. While Copernicus Publications makes every effort to include appropriate place names, the final responsibility lies with the authors.

Acknowledgements. The authors thank all the observational and reanalysis data providers used in this study and the research of the International Joint Laboratory "Dynamics of Terrestrial Ecosystems in Central Africa: A Context of Global Changes" (IJL DYCOCA/LMI DYCOFAC).

Review statement. This paper was edited by Martin Singh and reviewed by two anonymous referees.

References

Andrews, P. C., Cook, K. H., and Vizy, E. K.: Mesoscale convective systems in the Congo Basin: Seasonality, regionality, and diurnal cycles, Clim. Dynam., 62, 609–630, https://doi.org/10.1007/s00382-023-06903-7, 2023.

Aretouyap, Z., Kemgang, F. E. G., Domra, J. K., Bisso, D., and Njandjock, P. N.: Understanding the occurrences of fault and landslide in the region of West-Cameroon using remote sensing and GIS techniques, Nat. Hazards, 109, 1589–1602, https://doi.org/10.1007/s11069-021-04890-8, 2021.

Bell, J. P., Tompkins, A. M., Bouka-Biona, C., and Sanda, I. S.: A process-based investigation into the impact of the Congo basin deforestation on surface climate, J. Geophys. Res-Atmos., 120, 5721–5739, https://doi.org/10.1002/2014jd022586, 2015.

Black, E.: The relationship between Indian Ocean sea–surface temperature and East African rainfall, Philos. T. R. Soc. A, 363, 43–47, https://doi.org/10.1098/rsta.2004.1474, 2005.

Chen, J. and Bordoni, S.: Orographic effects of the Tibetan plateau on the east Asian summer monsoon: An energetic perspective, J. Climate, 27, 3052–3072, https://doi.org/10.1175/jcli-d-13-00479.1, 2014.

Cook, K. H. and Vizy, E. K.: Hydrodynamics of regional and seasonal variations in Congo Basin precipitation, Clim. Dynam., 59, 1775–1797, https://doi.org/10.1007/s00382-021-06066-3, 2021.

Cook, K. H., Liu, Y., and Vizy, E. K.: Congo Basin drying associated with poleward shifts of the African thermal lows, Clim. Dynam., 54, 863–883, https://doi.org/10.1007/s00382-019-05033-3, 2019.

Copernicus Climate Change Service (C3S): ERA5, Copernicus Climate Change Service [data set], https://cds.climate.copernicus.eu/datasets/reanalysis-era5-pressure-levels-monthly-means?tab=download, last access: 20 August 2024.

Dyer, E. L. E., Jones, D. B. A., Nusbaumer, J., Li, H., Collins, O., Vettoretti, G., and Noone, D.: Congo Basin precipitation: Assessing seasonality, regional interactions, and sources of moisture, J. Geophys. Res-Atmos., 122, 6882–6898, https://doi.org/10.1002/2016jd026240, 2017.

FloodList News: Kenya – over 100 dead, 18,000 displaced after recent floods and landslides – floodlist: http://floodlist.com/africa/kenya-floods-november-2019, last access: 2 April 2024.

Fontaine, B., Roucou, P., and Trzaska, S.: Atmospheric water cycle and moisture fluxes in the West African monsoon: Mean annual cycles and relationship using NCEP/NCAR reanalysis, Geophys. Res. Lett., 30, 3, https://doi.org/10.1029/2002gl015834, 2003.

Fotso-Nguemo, T. C., Chamani, R., Yepdo, Z. D., Sonkoué, D., Matsaguim, C. N., Vondou, D. A., and Tanessong, R. S.: Projected trends of extreme rainfall events from CMIP5 models over Central Africa, Atmos. Sci. Lett., 19, e803, https://doi.org/10.1002/asl.803, 2018.

Fotso-Nguemo, T. C., Diallo, I., Diakhaté, M., Vondou, D. A., Mbaye, M. L., Haensler, A., Gaye, A. T., and Tchawoua, C.: Projected changes in the seasonal cycle of extreme rainfall events from CORDEX simulations over Central Africa, Climatic Change, 155, 339–357, https://doi.org/10.1007/s10584-019-02492-9, 2019.

Funk, C., Peterson, P., Landsfeld, M., Pedreros, D., Verdin, J., Shukla, S., Husak, G., Rowland, J., Harrison, L., Hoell, A., and Michaelsen, J.: The climate hazards infrared precipitation with stations – a new environmental record for monitoring extremes, Scientific Data, 2, 150066, https://doi.org/10.1038/sdata.2015.66, 2015.

Garcin, Y., Deschamps, P., Ménot, G., de Saulieu, G., Schefuß, E., Sebag, D., Dupont, L. M., Oslisly, R., Brademann, B., Mbusnum, K. G., Onana, J.-M., Ako, A. A., Epp, L. S., Tjallingii, R., Strecker, M. R., Brauer, A., and Sachse, D.: Early anthropogenic impact on Western Central African rainforests 2,600 y ago, P. Natl. A. Sci. India. A, 115, 3261–3266, https://doi.org/10.1073/pnas.1715336115, 2018.

Gelaro, R., McCarty, W., Suárez, M. J., Todling, R., Molod, A., Takacs, L., Randles, C. A., Darmenov, A., Bosilovich, M. G., Reichle, R., Wargan, K., Coy, L., Cullather, R., Draper, C., Akella, S., Buchard, V., Conaty, A., da Silva, A. M., Gu, W., Kim, G.-K., Koster, R., Lucchesi, R., Merkova, D., Nielsen, J. E., Partyka, G., Pawson, S., Putman, W., Rienecker, M., Schubert, S. D., Sienkiewicz, M., and Zhao, B.: The Modern-Era Retrospective Analysis for Research and Applications, Version 2 (MERRA-2), J. Climate, 30, 5419–5454, https://doi.org/10.1175/jcli-d-16-0758.1, 2017.

Gou, Y., Balling, J., De Sy, V., Herold, M., De Keersmaecker, W., Slagter, B., Mullissa, A., Shang, X., and Reiche, J.: Intra-annual relationship between precipitation and forest disturbance in the African rainforest, Environ. Res. Lett., 17, 044044, https://doi.org/10.1088/1748-9326/ac5ca0, 2022.

Harris, I., Osborn, T. J., Jones, P., and Lister, D.: Version 4 of the CRU TS monthly high-resolution gridded multivariate climate dataset, Scientific Data, 7, 109, https://doi.org/10.1038/s41597-020-0453-3, 2020.

He, Y., Tian, W., Huang, J., Wang, G., Ren, Y., Yan, H., Yu, H., Guan, X., and Hu, H.: The mechanism of increasing summer water vapor over the Tibetan plateau, J. Geophys. Res-Atmos., 126, https://doi.org/10.1029/2020jd034166, 2021.

Hersbach, H., Bell, B., Berrisford, P., Hirahara, S., Horányi, A., Muñoz-Sabater, J., Nicolas, J., Peubey, C., Radu, R., Schepers, D., Simmons, A., Soci, C., Abdalla, S., Abellan, X., Balsamo, G., Bechtold, P., Biavati, G., Bidlot, J., Bonavita, M., De Chiara, G., Dahlgren, P., Dee, D., Diamantakis, M., Dragani, R., Flemming, J., Forbes, R., Fuentes, M., Geer, A., Haimberger, L., Healy, S., Hogan, R. J., Hólm, E., Janisková, M., Keeley, S., Laloyaux, P., Lopez, P., Lupu, C., Radnoti, G., de Rosnay, P., Rozum, I., Vamborg, F., Villaume, S., and Thépaut, J.: The ERA5 global reanalysis, Q. J. Roy. Meteor. Soc., 146, 1999–2049, https://doi.org/10.1002/qj.3803, 2020.

Hua, W., Zhou, L., Nicholson, S. E., Chen, H., and Qin, M.: Assessing reanalysis data for understanding rainfall climatology and variability over Central Equatorial Africa, Clim. Dynam., 53, 651–669, https://doi.org/10.1007/s00382-018-04604-0, 2019.

Huffman, G. J., Adler, R. F., Bolvin, D. T., and Gu, G.: Improving the global precipitation record: GPCP Version 2.1, Geophys. Res. Lett., 36, https://doi.org/10.1029/2009gl040000, 2009.

Jackson, B., Nicholson, S. E., and Klotter, D.: Mesoscale convective systems over Western Equatorial Africa and their relationship to large-scale circulation, Mon. Weather. Rev., 137, 1272–1294, https://doi.org/10.1175/2008mwr2525.1, 2009.

Jiang, J., Zhou, T., Chen, X., and Zhang, L.: Future changes in precipitation over Central Asia based on CMIP6 projections, Environ. Res. Lett., 15, 054009, https://doi.org/10.1088/1748-9326/ab7d03, 2020.

Johannsen, F., Ermida, S., Martins, J. P. A., Trigo, I. F., Nogueira, M., and Dutra, E.: Cold bias of ERA5 summertime daily maximum land surface temperature over Iberian Peninsula, Remote. Sens-Basel, 11, 2570, https://doi.org/10.3390/rs11212570, 2019.

Kamae, Y., Mei, W., and Xie, S.-P.: Climatological relationship between warm season atmospheric rivers and heavy rainfall over East Asia, J. Meteorol. Soc. Jpn., Ser. II, 95, 411–431, https://doi.org/10.2151/jmsj.2017-027, 2017.

Kenfack, K., Tamoffo, A. T., Djiotang Tchotchou, L. A., and Vondou, D. A.: Assessment of uncertainties in reanalysis datasets in reproducing thermodynamic mechanisms in the moisture budget's provision in the Congo Basin, Theor. Appl. Climatol., 154, 613–626, https://doi.org/10.1007/s00704-023-04576-0, 2023.

Kenfack, K., Tamoffo, A. T., Tchotchou, L. A. D., Marra, F., Kaissassou, S., Nana, H. N., and Vondou, D. A.: Processes behind the decrease in Congo Basin precipitation during the rainy seasons inferred from ERA-5 reanalysis, Int. J. Climatol., 44, i–iv, https://doi.org/10.1002/joc.8410, 2024.

Kuete, G., Pokam Mba, W., and Washington, R.: African Easterly Jet South: Control, maintenance mechanisms and link with Southern subtropical waves, Clim. Dynam., 54, 1539–1552, https://doi.org/10.1007/s00382-019-05072-w, 2019.

Li, P., Zhou, T., and Chen, X.: Water vapor transport for spring persistent rains over southeastern China based on five reanalysis datasets, Clim. Dynam., 51, 4243–4257, https://doi.org/10.1007/s00382-017-3680-3, 2017.

Liu, S., Wen, N., and Li, L.: Dynamic and thermodynamic contributions to Northern China dryness in El Niño developing summer, Int. J. Climatol., 41, 2878–2890, https://doi.org/10.1002/joc.6995, 2021.

Longandjo, G.-N. T. and Rouault, M.: Revisiting the seasonal cycle of rainfall over Central Africa, J. Climate, 37, 1015–1032, https://doi.org/10.1175/jcli-d-23-0281.1, 2024.

Lutz, K., Rathmann, J., and Jacobeit, J.: Classification of warm and cold water events in the eastern tropical Atlantic Ocean, Atmos. Sci. Lett., 14, 102–106, https://doi.org/10.1002/asl2.424, 2013.

Mariotti, L., Diallo, I., Coppola, E., and Giorgi, F.: Seasonal and intraseasonal changes of African monsoon climates in 21st century CORDEX projections, Climatic Change, 125, 53–65, https://doi.org/10.1007/s10584-014-1097-0, 2014.

Marra, F., Levizzani, V., and Cattani, E.: Changes in extreme daily precipitation over Africa: Insights from a non-asymptotic statistical approach, J. Hydrol. X, 16, 100130, https://doi.org/10.1016/j.hydroa.2022.100130, 2022.

Moon, S. and Ha, K.-J.: Future changes in monsoon duration and precipitation using CMIP6, NPJ Clim. Atmos. S., 3, 45, https://doi.org/10.1038/s41612-020-00151-w, 2020.

Moudi Pascal, I., Kammalac Jores, T., Talib, J., Appolinaire, V. D., Hirons, L., Christian, N., Tene Romeo-Ledoux, D., Fogang Michael, T., Marceline, M., Tanessong Roméo, S., Dione, C., Thompson, E., Salih, A. A. M., and Ngaryamgaye, S.: Strengthening weather forecast and dissemination capabilities in Central Africa: Case assessment of intense flooding in January 2020, Climate Services, 32, 100411, https://doi.org/10.1016/j.cliser.2023.100411, 2023.

Nana, H. N., Tanessong, R. S., Tchotchou, L. A. D., Tamoffo, A. T., Moihamette, F., and Vondou, D. A.: Influence of strong South Atlantic Ocean Dipole on the Central African rainfall's system, Clim. Dynam., 62, 1–16, https://doi.org/10.1007/s00382-023-06892-7, 2023.

NCAR Command Language: UCAR/NCAR/CISL/TDD [software], Boulder, Colorado, https://doi.org/10.5065/D6WD3XH5, 2017.

Neelin, J. D.: Moist dynamics of tropical convection zones in monsoons, teleconnections, and global warming, in: The Global Circulation of the Atmosphere, Princeton University Press, 267–301, 2021.

Ngandam Mfondoum, A. H., Wokwenmendam Nguet, P., Mefire Mfondoum, J. V., Tchindjang, M., Hakdaoui, S., Cooper, R., Gbetkom, P. G., Penaye, J., Bekoa, A., and Moudioh, C.: Adapting sudden landslide identification product (SLIP) and detecting real-time increased precipitation (DRIP) algorithms to map rainfall-triggered landslides in Western Cameroon highlands (Central-Africa), Geoenvironmental Disasters, 8, 17, https://doi.org/10.1186/s40677-021-00189-9, 2021.

Nicholson, S. E., Fink, A. H., Funk, C., Klotter, D. A., and Satheesh, A. R.: Meteorological causes of the catastrophic rains of October/November 2019 in equatorial Africa, Global. Planet. Change, 208, 103687, https://doi.org/10.1016/j.gloplacha.2021.103687, 2022.

Oueslati, B., Yiou, P., and Jézéquel, A.: Revisiting the dynamic and thermodynamic processes driving the record-breaking January 2014 precipitation in the southern UK, Sci. Rep.-UK, 9, 2859, https://doi.org/10.1038/s41598-019-39306-y, 2019.

Pokam, W. M., Djiotang, L. A. T., and Mkankam, F. K.: Atmospheric water vapor transport and recycling in Equatorial Central Africa through NCEP/NCAR reanalysis data, Clim. Dynam., 38, 1715–1729, https://doi.org/10.1007/s00382-011-1242-7, 2011.

Pokam, W. M., Bain, C. L., Chadwick, R. S., Graham, R., Sonwa, D. J., and Kamga, F. M.: Identification of processes driving low-level westerlies in West Equatorial Africa, J. Climate, 27, 4245–4262, https://doi.org/10.1175/jcli-d-13-00490.1, 2014.

Reed, R. J., Norquist, D. C., and Recker, E. E.: The Structure and Properties of African Wave Disturbances as Observed During Phase III of GATE, Mon. Weather Rev., 105, 317–333, https://doi.org/10.1175/1520-0493(1977)105<0317:tsapoa>2.0.co;2, 1977.

Seager, R., Naik, N., and Vecchi, G. A.: Thermodynamic and dynamic mechanisms for large-scale changes in the hydrological cycle in response to global warming, J. Climate, 23, 4651–4668, https://doi.org/10.1175/2010jcli3655.1, 2010.

Sheng, B., Wang, H., Li, H., Wu, K., and Li, Q.: Thermodynamic and dynamic effects of anomalous dragon boat water over South China in 2022, Weather and Climate Extremes, 40, 100560, https://doi.org/10.1016/j.wace.2023.100560, 2023.

Sonkoué, D., Monkam, D., Fotso-Nguemo, T. C., Yepdo, Z. D., and Vondou, D. A.: Evaluation and projected changes in daily rainfall characteristics over Central Africa based on a multi-model ensemble mean of CMIP5 simulations, Theor. Appl. Climatol., 137, 2167–2186, https://doi.org/10.1007/s00704-018-2729-5, 2018.

Taguela, T. N., Pokam, W. M., and Washington, R.: Rainfall in uncoupled and coupled versions of the Met Office Unified Model over Central Africa: Investigation of processes during the September–November rainy season, Int. J. Climatol., 42, 6311–6331, https://doi.org/10.1002/joc.7591, 2022.

Tamoffo, A. T., Vondou, D. A., Pokam, W. M., Haensler, A., Yepdo, Z. D., Fotso-Nguemo, T. C., Tchotchou, L. A. D., and Nouayou, R.: Daily characteristics of Central African rainfall in the REMO model, Theor. Appl. Climatol., 137, 2351–2368, https://doi.org/10.1007/s00704-018-2745-5, 2019.

Tamoffo, A. T., Dosio, A., Weber, T., and Vondou, D. A.: Dynamic and Thermodynamic Contributions to Late 21st Century Projected Rainfall Change in the Congo Basin: Impact of a Regional Climate Model's Formulation, Atmosphere-Basel, 14, 1808, https://doi.org/10.3390/atmos14121808, 2023a.

Tamoffo, A. T., Weber, T., Akinsanola, A. A., and Vondou, D. A.: Projected changes in extreme rainfall and temperature events and possible implications for Cameroon's socio-economic sectors, Meterol. Appl., 30, https://doi.org/10.1002/met.2119, 2023b.

Tamoffo, A. T., Weber, T., Cabos, W., Sein, D. V., Dosio, A., Rechid, D., Remedio, A. R., and Jacob, D.: Mechanisms of Added Value of a Coupled Global Ocean-Regional Atmosphere Climate Model Over Central Equatorial Africa, J. Geophys Res-Atmos., 129, https://doi.org/10.1029/2023jd039385, 2024.

Vallès-Casanova, I., Lee, S., Foltz, G. R., and Pelegrí, J. L.: On the Spatiotemporal Diversity of Atlantic Niño and Associated Rainfall Variability Over West Africa and South America, Geophys. Res. Lett., 47, https://doi.org/10.1029/2020gl087108, 2020.

Wainwright, C. M., Finney, D. L., Kilavi, M., Black, E., and Marsham, J. H.: Extreme rainfall in East Africa, October 2019–January 2020 and context under future climate change, Weather, 76, 26–31, https://doi.org/10.1002/wea.3824, 2020.

Wang, L. and Li, T.: Effect of vertical moist static energy advection on MJO eastward propagation: Sensitivity to analysis domain, Clim. Dynam., 54, 2029–2039, https://doi.org/10.1007/s00382-019-05101-8, 2020a.

Wang, T. and Li, T.: Diagnosing the column-integrated moist static energy budget associated with the northward-propagating boreal summer intraseasonal oscillation, Clim. Dynam., 54, 4711–4732, https://doi.org/10.1007/s00382-020-05249-8, 2020b.

Wantim, M. N., Ughe, W. G., Kwah, D. C., Bah, T. C., Quinette, N., and Ayonghe, S. N.: Forensic investigation of the Gouache landslide disaster, Western Region, Cameroon, Journal of the Cameroon Academy of Sciences, 19, 223–240, https://doi.org/10.4314/jcas.v19i3.3, 2023.

Washington, R., James, R., Pearce, H., Pokam, W. M., and Moufouma-Okia, W.: Congo Basin rainfall climatology: Can we believe the climate models?, Philos. T. R. Soc. B., 368, 20120296, https://doi.org/10.1098/rstb.2012.0296, 2013.

Wen, N., Liu, S., and Li, L. Z. X.: Diagnosing the dynamic and thermodynamic effects for the exceptional 2020 summer rainy season in the Yangtze River Valley, J. Meteorol. Res-Prc., 36, 26–36, https://doi.org/10.1007/s13351-022-1126-2, 2022.

Yanai, M. and Tomita, T.: Seasonal and interannual variability of atmospheric heat sources and moisture sinks as determined from NCEP–NCAR reanalysis, J. Climate, 11, 463–482, https://doi.org/10.1175/1520-0442(1998)011<0463:saivoa>2.0.co;2, 1998.

Zhao, D., Zhang, L., and Zhou, T.: Detectable anthropogenic forcing on the long-term changes of summer precipitation over the Tibetan Plateau, Clim. Dynam., 59, 1939–1952, https://doi.org/10.1007/s00382-022-06189-1, 2022.

Zhou, L., Tian, Y., Myneni, R. B., Ciais, P., Saatchi, S., Liu, Y. Y., Piao, S., Chen, H., Vermote, E. F., Song, C., and Hwang, T.: Widespread decline of Congo rainforest greenness in the past decade, Nature, 509, 86–90, https://doi.org/10.1038/nature13265, 2014.